Practical Limitation on Operation of Nonlinear Parity-Time Bragg Gratings

Sendy Phang[1,*], Ana Vukovic[1], Hadi Susanto[2], Trevor M. Benson[1], and Phillip Sewell[1]

[1]The George Green Institute for Electromagnetics Research, Faculty of Engineering, University of Nottingham, Nottingham NG7 2RD UK
[2]Department of Mathematical Sciences, University of Essex, Colchester CO4 3SQ, UK
*corresponding author, E-mail: sendy.phang@nottingham.ac.uk

Abstract

The paper analyses the operation of PT Bragg gratings when the dielectric material is considered to be both dispersive and nonlinear and gain and loss are saturable. The paper demonstrates the application of the nonlinear PT Bragg Grating as an optical logic gate and an optical switch.

1. Introduction

A Parity-Time (PT) structure is formed by balancing inherent loss in a medium by an equal gain in a certain design. The PT-symmetric structures mimic the PT-symmetric potential system in quantum physics which, under certain conditions, operates in a stable regime. As optical waveguides have inherent material loss, it is desirable to balance the loss with gain for optimal performance. This is one of the reasons why PT structures have become the subject of increased interest in photonics. Several kinds of PT-symmetric structures have been reported so far based on either grating [1–4], coupler [5–9], or lattice [10–12] structures with a range of applications including lasing and absorber cavities [2], switches [4,13] and memory [14]. PT-structures have been extensively modelled using coupled-mode theory [3,7], the transfer-matrix (T-matrix) method [1,14–16], Floquet-Bloch theory [11] and Fourier modal analysis [17,18]. The inclusion of material nonlinearity has also been reported with a speculation that nonlinearity combined with a PT structure will open a new range of functionalities [1,19–21]. However, all the reported models have assumed that gain and loss are frequency and intensity independent. The important question arises on how a nonlinear PT-symmetric device will perform in a practical situation where gain and loss are both dispersive and saturable, especially when medium nonlinearity is also taken into account.

To consider such a scenario we use a time-domain numerical technique, namely the Transmission Line Modelling (TLM) method [22,23]. The TLM method is based upon the analogy between the propagating electromagnetic field and voltage impulses travelling on an interconnected mesh of transmission lines. Successive repetitions of a scatter-propagate procedure provide an explicit and stable time-stepping-algorithm that mimics electromagnetic field behaviour to second order accuracy in both time and space [24,25]. It is important to note that the TLM method has been successfully implemented to model a dispersive and nonlinear dielectric material [22,23]. In principle any time-domain numerical method, including the Finite Difference Time Domain (FDTD) method could be used as a basis for the simulation undertaken.

In our previous work, we have validated the TLM method to model a linear PT Bragg Grating (PTBG) with non-dispersive gain and loss [4,26]. The impact of gain/loss saturation on the switching performance of a linear PTBG, has also been demonstrated [4]. In this paper we extend our model to include nonlinear and dispersive materials with saturable gain and loss. The Kerr nonlinearity is assumed in this paper and is controlled by a strong pump beam away from the Bragg frequency of the grating. The performance of the grating for different pump beam intensities and different saturation intensities is analysed. This is followed by studies of the applications of a nonlinear PTBG as an optical logic gate and a switch.

This paper is structured as follows; in the next section the model of the PTBG structure as implemented in the TLM method is given. Section 3 analyses the performance of the nonlinear PTBG for different input intensities and different intensity saturation levels. Section 4 demonstrates practical applications of the nonlinear PTBG and Section 5 outlines the main conclusions of the paper.

2. Structure and model

A Parity-Time symmetric material in optics requires a complex refractive index profile that satisfies $\hat{n}(-z) = \hat{n}^*(z)$, where z denotes the spatial position of the grating and * denotes the complex conjugate. The schematic of a PT grating is shown in Fig. 1. The grating is embedded in a medium of background refractive index n_B as shown in Fig. 1(a), and is made of N periods. A single period, Λ, of the PTBG is shown in Fig. 1(b) representing equal amounts of loss and gain per period and with the real refractive index varying in a piecewise constant manner between n_L and n_H (dashed line in Fig. 1(b)). The Bragg frequency f_B is related to the average refractive index $\bar{n}$ of the structure by $f_B = \frac{c}{2\bar{n}\Lambda}$, where c is the speed of light in free space.

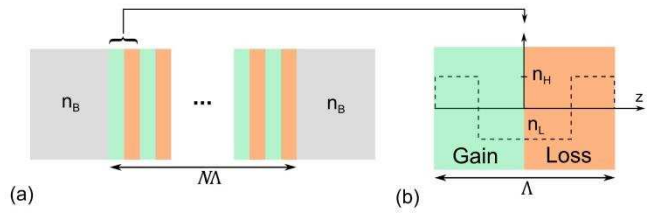

Fig. 1(a) Schematic of the PTBG within a background material n_B; (b) A single period of PTBG showing gain and loss half-periods and (dashed line) modulation of the real refractive index.

The refractive index profile of the nonlinear PT Bragg grating for one period n_G can be expressed as:

$$n_G(z,\omega,t,I) = \begin{cases} n(\omega) \pm \Delta n(z) + n_2 I(z,t) + j\frac{c}{\omega}\alpha(\omega,I), & z < \frac{\Lambda}{2} \\ n(\omega) \mp \Delta n(z) + n_2 I(z,t) - j\frac{c}{\omega}\alpha(\omega,I), & z > \frac{\Lambda}{2} \end{cases} \quad (1)$$

Here, $n(\omega)$ is the base refractive index as a frequency dependent material, $\Delta n(x)$ is the modulation of the real refractive index as a spatially dependent function, n_2 is the Kerr nonlinearity constant, I is the input intensity of the field and $\alpha(\omega, I)$ denotes gain or loss in the grating which is dispersive and saturable. Equation (1) shows that Kerr nonlinearity also contributes to the overall real part of the refractive index.

The frequency and intensity dependent dielectric material is modelled in the TLM model using the Duffing equation of polarisation [27],

$$\frac{\partial^2 P_D}{\partial t^2} + 2\delta\frac{\partial P_D}{\partial t} + \omega_{0D}^2 P_D f_D = \epsilon_0 \chi_{e0}\omega_{0D}^2 E \quad (2)$$

where P_D and E denote the electric polarisation and field, δ and ω_{0D} denote the damping and dielectric resonant angular-frequency parameters of the medium respectively, and χ_{e0} denotes the dielectric susceptibility at DC. The nonlinearity is implemented with the function f_D as [28],

$$f_D = e^{\zeta P_D^2}, \quad (3)$$

where $\zeta = -\frac{n_2\sqrt{\chi_{e0}+\chi_{e\infty}+1}}{\epsilon_0^2(\chi_{e0}+\chi_{e\infty})^3\eta_0}$, n_2 is the Kerr nonlinear constant, $\chi_{e\infty}$ denotes the constant susceptibility at infinite frequency and η_0 is the free-space impedance. It is emphasised that when $f_D = 1$ the Duffing equation reduces to the linear model of optical material based on simple harmonic oscillator with a Lorentzian profile. In this case the refractive index at a given angular frequency ω is calculated as,

$$\hat{n}^2 = (1+\chi_{e\infty}) + \frac{\chi_{e0}\omega_{0D}^2}{2j\delta\omega+(\omega_{0D}^2-\omega^2)}. \quad (4)$$

The implementation and validation of the Duffing equation to model a realistic dispersive and nonlinear optical dielectric has been reported in [28].

On the other hand, a dispersive and saturable gain/loss model with a Lorentzian profile is implemented as [29],

$$|\alpha|(\omega,I) = \Omega(I)\left(\frac{\alpha_0}{1+j(\omega-\omega_{0\sigma})\tau} + \frac{\alpha_0}{1+j(\omega+\omega_{0\sigma})\tau}\right), \quad (5)$$

where the gain/loss parameter $|\alpha|$ is related with the imaginary part of refractive index n_I by $|\alpha| = \frac{\omega}{c}n_I$, $\omega_{0\sigma}$ denotes the atomic transition angular-frequency, τ is the dipole relaxation time parameter and α_0 is the peak value of the gain or loss at $\omega_{0\sigma}$. In order to quantify the saturation level, it is useful to introduce the saturation factor Ω defined as,

$$\Omega = \frac{1}{1+\frac{I}{I_S}}, \quad (6)$$

where I is the input beam intensity and I_S is the saturation intensity. For a fixed I_S, the saturation factor Ω varies over the interval $0 < \Omega < 1$, with $\Omega = 0$ denoting a highly saturated state ($\frac{I}{I_S} \to \infty$) and $\Omega = 1$ denoting negligible saturation ($\frac{I}{I_S} \to 0$). It is emphasised that the model described in (2)-(6) satisfies the Kramers-Kronigs conditions which relates the real and imaginary part of a refractive index.

3. Results and Discussion

In this section, the performance of 200 periods of nonlinear PTBG based on GaAs material is analysed using the TLM method. The following material parameters are used throughout this paper, $\chi_{e0} = 7.5$, $\omega_{0D} = 4614.4\ \text{rad/ps}$, and $\delta = 0.0923\ \text{rad/ps}$ [30], with the high and low refractive index, i.e. n_H and n_L obtained respectively from the high and low dielectric susceptibilities, $\chi_{e\infty} = 2.8$ and 2.5, which form the grating. The Kerr nonlinearity constant is $n_2 = 2\times10^{-17}\ \text{m}^2\text{W}^{-1}$ [31,32] throughout the structure. The gain and loss parameters are $\tau = 0.1$ ps and $\omega_{0\sigma} = 2116.5\ \text{rad/ps}$ [29] while α_0 depends on the gain/loss given. The periodicity of the PTBG is designed so that the Bragg frequency is at the atomic-transitional frequency, i.e. $f_B = \frac{\omega_{0\sigma}}{2\pi}$, hence $\Lambda = 122.7$ nm. The background material is GaAs with $n_B = 3.626$ at the Bragg frequency f_B. The unidirectional (U) operation of the PTBG occurs when the gain/loss in the PTBG satisfies $|\alpha_0| = \frac{1\omega}{2c}(n_H - n_L)$ [4] which for the chosen material parameters, happens when the gain/loss coefficient $|\alpha_0| = 1460.24\ \text{cm}^{-1}$.

The main characteristic of the linear PT Bragg grating is that transmission is the same regardless of whether the grating is excited from the left or right of the grating but the reflectances are different. The amount of gain/loss of the system also influences the operation of the grating in that above a certain threshold point the operation of grating is in an unstable regime. Another characteristic of a linear PTBG is that the grating exhibits unidirectional invisibility – commonly referred to as the U point.

In the light of the refractive index profile given in (1), for the nonlinear PT Bragg grating, we consider a scenario where an input beam is comprised of two beams, namely a strong pump beam and a probe beam. The pump beam is a CW beam and is used to activate the Kerr nonlinearity. The frequency of the pump beam f_{pump} is set to be far from the Bragg frequency, i.e. $f_{pump} = 200$ THz. The probe signal is a Gaussian pulse modulated at the Bragg frequency f_B and is low in intensity, with its maximum intensity being 1% of

the pump beam intensity. Since the intensity of probe beam is very low compared to the strong pump beam, its effect can be seen as a perturbation of the pump beam and hence the pump beam can be considered as the input beam.

In order to investigate the effect of different saturation levels on the performance of a nonlinear PTBG the saturation intensity I_S is fixed to a certain level and the saturation factor Ω is changed by changing the intensity of the pump beam.

Fig. 2 shows the frequency response of the nonlinear PTBG for a saturation intensity $I_S = 5 \times 10^{10}$ Wm^{-2} at the U-point. For a given level of saturation intensity, the effect of the Kerr nonlinearity is low since $n_2 I_S = 1 \times 10^{-6}$. Four different intensities of the input beam I are considered so that the saturation factor Ω varies from low to high saturation, i.e. $\Omega = 0.99,\ 0.8,\ 0.01$ and 2×10^{-6}. Fig. 2 compares results together with the analytical solution obtained using the T-matrix method [34]. It is emphasised here, that the T-matrix method models a linear and dispersive structure, i.e. no Kerr nonlinearity and no gain/loss saturation. With that in mind, the T-matrix method results are presented more as a reference than for a direct comparison. The response of the linear PTBG using the idealised model of gain/loss [1] is also included in Fig. 2 for comparison. The ideal gain/loss model here is implied to be frequency and intensity independent.

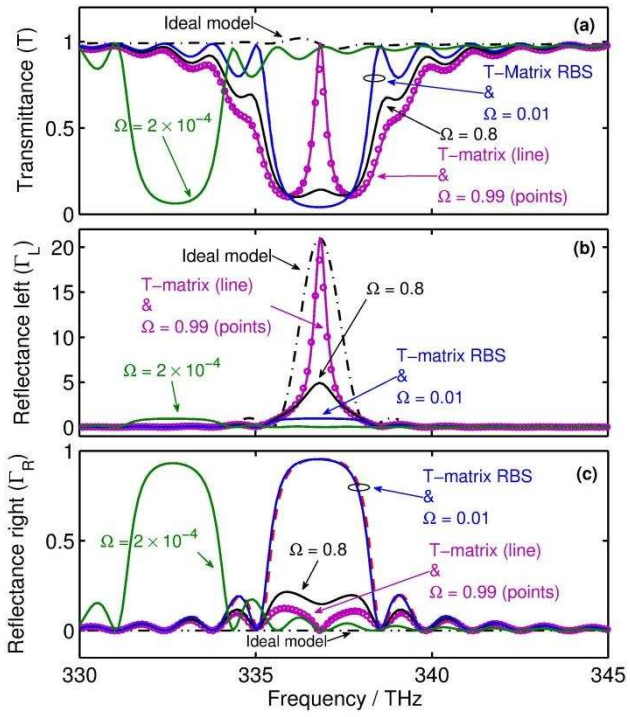

Fig. 2(a)Transmittance (b) reflectance for left, Γ_L , and (c) right, Γ_R, incident for different saturation levels Ω

Fig. 2(a) shows that transmittance of the ideal PTBG model has almost-total transmission $T \approx 1$ at all frequencies. At low saturation level ($\Omega = 0.99$), the transmittance calculated using the TLM method agrees with one calculated with the T-matrix method, due to the fact that in this case the change of refractive index and gain/loss in the PTBG induced by the Kerr nonlinearity and saturation respectively are negligible. It is noticeable that compared to the idealised case, the total transmission $T = 1$ occurs only at the Bragg frequency f_B. This result confirms that material dispersion prohibits unidirectional behaviour at all frequencies as shown in the case of an ideal PTBG [4]. Furthermore, as the saturation factor Ω decreases the transmittance becomes similar to that of the regular Bragg grating (RBG), i.e. it loses PT behaviour. This is shown in Fig. 2(a) where the response for $\Omega = 0.01$ overlaps with that of the RBG. By increasing the input beam intensity even further, $\Omega = 2 \times 10^{-4}$, the band-gap is shifted to the lower frequency due to the fact that the dominant modulation mechanism becomes the Kerr nonlinearity.

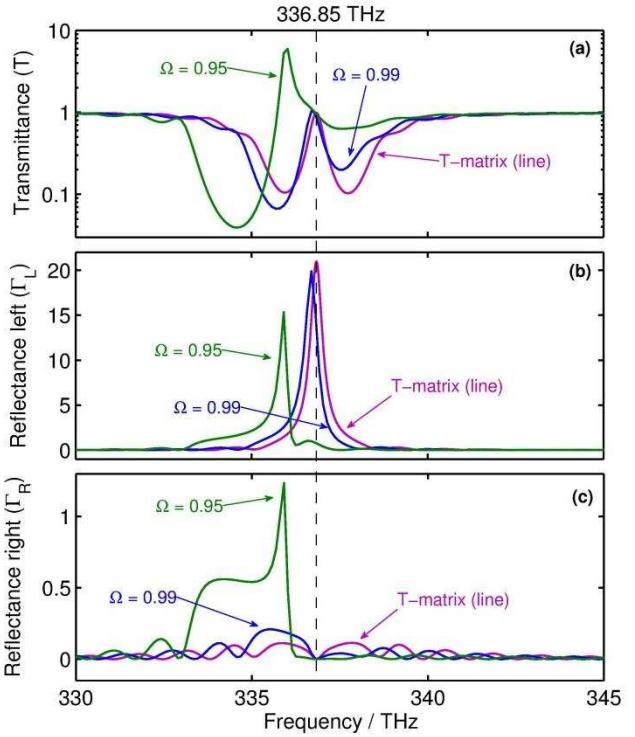

Fig. 3(a)Transmittance (b) reflectance for left Γ_L and (c) right Γ_R incident beam for high saturation intensity and different saturation factors Ω

Fig. 2(b) and Fig. 2(d) show the reflectance for beams incident from the left, Γ_L, and right, Γ_R, side of the PTBG respectively. For the ideal linear PTBG the reflectance Γ_R is zero and Γ_L is amplified, showing the unidirectional behaviour at all frequencies. At low saturation levels ($\Omega = 0.99$) the reflectance Γ_L has narrower bandwidth and the PTBG maintains the unidirectional behaviour around f_B. Furthermore, at low saturation, $\Omega = 0.99$, the TLM results for Γ_L and Γ_R agree very well with results obtained using the T-matrix method due to the negligible effect of nonlinearity. Further increase in saturation level shifts the reflectance spectra to lower frequencies due to the dominant Kerr nonlinearity.

Fig. 3(a) shows the response of the nonlinear PTBG

under the condition of high saturation intensity, which if it was reached, produces high Kerr nonlinearity of $n_2 I_S = 0.5$. The grating is operated at the U point with $|\alpha_0| = 1460.24$ cm^{-1}. Two different input intensities are considered so that gain/loss saturation is $\Omega = 0.99$ and 0.95, corresponding to low saturation. The induced Kerr modulation for given intensities is $n_2 I = 0.0051$ and 0.0263 respectively. The response of the linear structure (no Kerr nonlinearity and no gain/loss saturation) calculated using the T-matrix method is included for comparison. Fig. 3 shows that as the intensity and saturation increase the overall responses for T, Γ_R and Γ_L shift towards lower frequencies as the Kerr nonlinearity increases overall refractive index. It is observed that at the f_B the unidirectional invisibility is preserved, $T \approx 1$ and $\Gamma_R \to 0$, whilst transmittance higher than 1 is observed for $f < f_B$. The reflectance for the left incident case, Γ_L, decreases and is shifted to a lower frequency. On the other hand, the Γ_R increases as the input beam increases and negligible reflectance is observed for $f > f_B$.

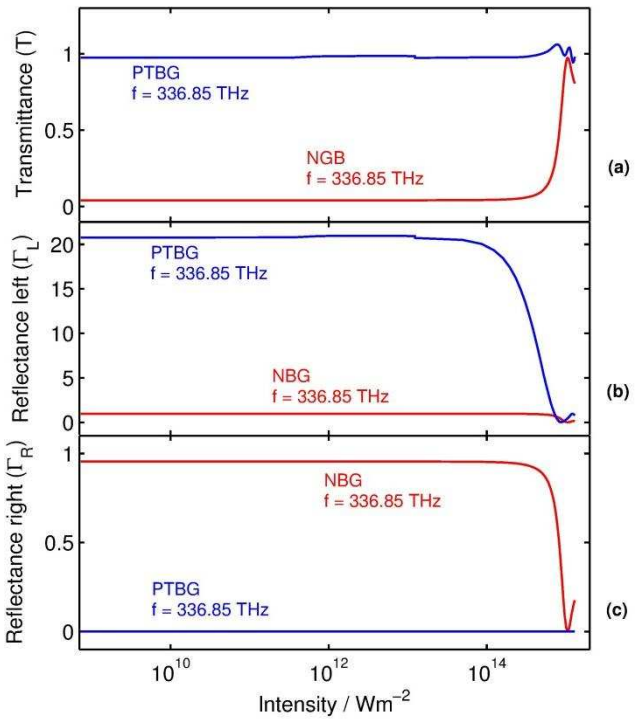

Fig. 4 (a) Transmittance, (b) reflectance for left and (c) reflectance for right of PTBG at the U operation as a function of input intensity at $f = 336.85$ THz. The gain/loss has high saturation intensity $n_2 I_S = 0.5$. Results for the NBG($\alpha_0 = 0$) at the Bragg frequency $f_B = 336.85$ THz are included for reference.

Fig. 4 shows the response of the nonlinear PTBG as a function of input beam intensity, when the gain/loss intensity saturation is high $(n_2 I_S = 0.5)$. The grating is operated at the U point with $f = 336.85$ THz. The frequency $f = 336.85$ THz is the Bragg frequency of the linear grating. The response for the nonlinear Bragg grating (NBG) at $f = 336.85$ THz , with no gain and loss $(\alpha_0 = 0)$ is also included in Fig. 4(a) and shows that at low intensities the transmittance is very low but then switches to total transmittance at high intensity. This can be explained that by the fact that at high input intensity the band-gap of the nonlinear Bragg grating is shifted to the lower frequency so that $f = 336.85$ THz lies outside the band-gap. For the case of the nonlinear PTBG operating at $f = 336.85$ THz, the total transmission $T = 1$ is achieved regardless of the input beam intensity.

Since the NBG is orthogonal (reciprocal and lossless), i.e. $T + \Gamma = 1$, Fig. 4(b,c) show that at low input intensity the reflectance is close to 1, and it is very small at high input intensity. For the case of a nonlinear PTBG the reflectance, $\Gamma_L \neq \Gamma_R$ with $\Gamma_L > \Gamma_R$ at low input intensity, i.e. small Kerr effect, but as the input intensity increases the Γ_L decreases to almost zero and fits with the response of the NBG. Fig. 4(a,b) show that at high input intensity and for high saturation intensity, total transmittance with both $\Gamma_L, \Gamma_R \to 0$ is observed corresponding to a bidirectionally transparent grating for frequencies $f > f_B$.

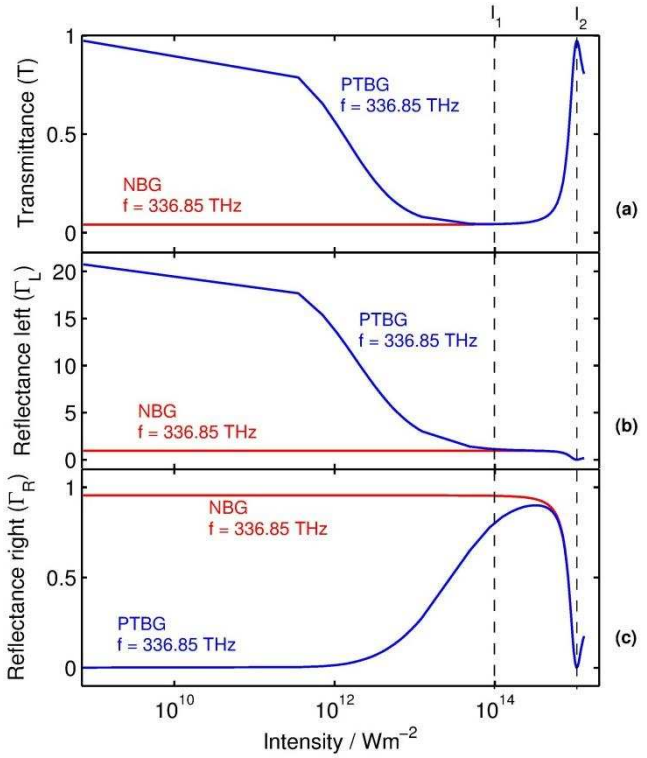

Fig. 5 (a) Transmittance, (b) reflectance for left and (c) reflectance for right incidence of PTBG at the U operation as a function of input intensity at $f = 336.85$ THz. The gain/loss has low saturation intensity $n_2 I_S = 0.0005$. Results for the NBG $(\alpha_0 = 0)$ at the Bragg frequency $f_B = 336.85$ THz are included for reference.

The impact of gain/loss saturation on the performance of the nonlinear PTBG as a function of input beam intensity is shown in Fig. 5. The grating is operated at $f = 336.85$ THz, similarly as in Fig. 4. The saturation intensity is low and set to $I_S = 2.5 \times 10^{13}$ Wm^{-2}, corresponding to a low Kerr nonlinearity of $n_2 I_S = 0.0005$. The PTBG operates at

the U point with $|\alpha_0| = 1460.24\ \mathrm{cm}^{-1}$. Fig. 5(a) shows almost total transmittance at low input intensity but it gradually decreases and fits with the response of the NBG as the input intensity is increased.

Fig. 5(b) and (c) depict the reflectance for the left Γ_L and right Γ_R incidence respectively. At low input intensity $\Gamma_L > \Gamma_R$, but it gradually decreases and fits with the response of the NBG as the input intensity is increased. Fig. 5(a-c) show the impact of the gain/loss saturation, that it effectively reduces the gain/loss in the system to a negligible level at high input intensity, and hence inhibits the interplay of Kerr nonlinearity and PT behaviour as is observed in Fig. 4.

4. Applications

In this section two potential applications of a nonlinear PTBG based on GaAs are investigated, namely an optical logic gate and a switch. The input beam comprises of a probe beam and a strong pump beam. The probe beam is a CW operated at the Bragg frequency $f_{probe} = 336.85$ THz and has a low intensity which is kept constant throughout the simulation with $I = 1 \times 10^6\ \mathrm{Wm}^{-2}$. The pump beam is a CW signal operated far from the Bragg frequency at $f_{pump} = 200$ THz. The intensities of the pump beam are switched between two different values, i.e. $I_1 = 1 \times 10^{14}\ \mathrm{Wm}^{-2}$ and $I_2 = 1 \times 10^{15}\mathrm{Wm}^{-2}$ as marked in Fig. 5, where the pump beam intensity is shown against time. The pump beam is initially turned off and then turned on to intensity I_1 for a duration of 10 ps, followed by an increase to intensity I_2 for another 10 ps. The pattern is then repeated as seen in Fig. 6(a).

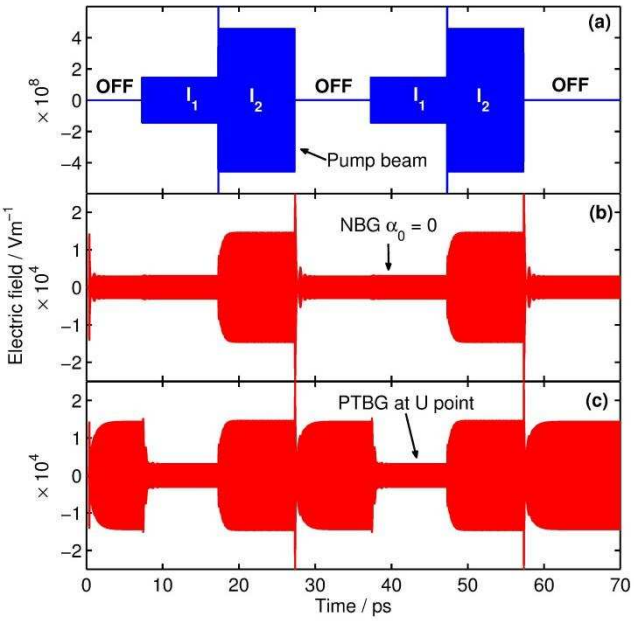

Fig. 6 Comparison of switching operation between the (b) NBG and (c) PTBG for the pump beam intensity profile shown in (a).

Fig. 6 compares the performance of the NBG and PTBG where Fig. 6(b) shows the transmitted probe beam of a NBG structure ($\alpha_0 = 0$) when excited from the left side. The transmitted probe beam of the NBG is very low when the pump beam is turned off or operated at $I = I_1$. However, when the pump beam is switched to operate at I_2 total transmitted power is observed. On the other hand, Fig. 6(c) shows the output of the PTBG when the grating is excited from the left. It can be seen that when the pump beam is off the probe beam is totally transmitted $T = 1$. Increase in the pump beam intensity to I_1 reduces the transmitted probe beam intensity. A subsequent further increase of the pump beam to I_2 increases the transmitted probe beam to total transmittance. Although Fig. 6(b) and Fig. 6(c) show that NBG and PTBG have similar switching operation, the PTBG achieves switching at lower pump intensity with the default ON state for $I = 0$ and OFF state at $I = I_1$.

5. Conclusion

The performance of a nonlinear PT Bragg grating that has dispersive material and a saturable gain/loss model is analysed and compared with the performance of an idealised PT Bragg grating and a nonlinear Bragg grating with no gain/loss. It is shown that material dispersion limits the unidirectional behaviour of the PTBG to a narrowband region around the Bragg frequency. The interplay of saturation and nonlinearity is important as low saturation intensity can prohibit the impact of Kerr nonlinearity in a nonlinear PTBG. At high saturation intensity the impact of nonlinearity contributes to bidirectional invisibility for frequencies above the Bragg frequency. The operation of the PTBG as an optical switch and logic gate confirms that the switching operation can be achieved at lower pump intensities than is the case for the nonlinear Bragg grating with no gain and loss.

References

1. Z. Lin, H. Ramezani, T. Eichelkraut, T. Kottos, H. Cao, and D. N. Christodoulides, "Unidirectional Invisibility Induced by PT-Symmetric Periodic Structures," Physical Review Letters 106, 213901 (2011).
2. Y. D. Chong, L. Ge, and a. D. Stone, "PT-symmetry breaking and laser-absorber modes in optical scattering systems," Physical Review Letters 106, 093902 (2011).
3. M. Kulishov, J. M. Laniel, N. Bélanger, J. Azaña, and D. V Plant, "Nonreciprocal waveguide Bragg gratings," Optics Express 13, 3068–78 (2005).
4. S. Phang, A. Vukovic, H. Susanto, T. M. Benson, and P. Sewell, "Ultrafast optical switching using parity–time symmetric Bragg gratings," Journal of the Optical Society of America B 30, 2984 (2013).
5. M. Greenberg and M. Orenstein, "Unidirectional complex grating assisted couplers.," Optics Express 12, 4013–8 (2004).
6. T. Kottos, "Optical physics: Broken symmetry makes light work," Nature Physics 6, 166–167 (2010).

7. R. El-Ganainy, K. G. Makris, D. N. Christodoulides, and Z. H. Musslimani, "Theory of coupled optical PT-symmetric structures," Optics Letters 32, 2632 (2007).
8. L. Chen, R. Li, N. Yang, D. Chen, and L. Li, "Optical modes in PT-Symmetric double-Channel waveguides," arXiv preprint arXiv: 1202.2956 (2012).
9. C. E. Rüter, K. G. Makris, R. El-Ganainy, D. N. Christodoulides, M. Segev, and D. Kip, "Observation of parity–time symmetry in optics," Nature Physics 6, 192–195 (2010).
10. A. Regensburger, C. Bersch, M.-A. Miri, G. Onishchukov, D. N. Christodoulides, and U. Peschel, "Parity-time synthetic photonic lattices - Supplementary method.," Nature 488, 167–71 (2012).
11. K. G. Makris, R. El-Ganainy, and D. N. Christodoulides, "Beam dynamics in PT symmetric optical lattices," Physical Review Letters 100, 103904 (2008).
12. S. Nixon, L. Ge, and J. Yang, "Stability analysis for solitons in PT-symmetric optical lattices," Physical Review A 85, 023822 (2012).
13. F. Nazari, M. Nazari, and M. K. Moravvej-Farshi, "A 2×2 spatial optical switch based on PT-symmetry.," Optics Letters 36, 4368–70 (2011).
14. M. Kulishov, B. Kress, and R. Slavík, "Resonant cavities based on Parity-Time-symmetric diffractive gratings," Optics Express 21, 68–70 (2013).
15. A. Mostafazadeh, "Invisibility and PT symmetry," Physical Review **A** 11 (2013).
16. A. Mostafazadeh, "Spectral singularities of complex scattering potentials and infinite reflection and transmission coefficients at real energies," Physical Review Letters 102, 220402 (2009).
17. J. Čtyroký, V. Kuzmiak, and S. Eyderman, "Waveguide structures with antisymmetric gain/loss profile," Optics Express 18, 21585–21593 (2010).
18. J. Čtyroký, "Dispersion properties of coupled waveguides with loss and gain: a full-vectorial analysis," Optical and Quantum Electronics (2014).
19. H. Ramezani, T. Kottos, R. El-Ganainy, and D. N. Christodoulides, "Unidirectional nonlinear PT-symmetric optical structures," Physical Review **A** 82, 043803 (2010).
20. Z. Musslimani, K. Makris, R. El-Ganainy, and D. N. Christodoulides, "Optical solitons in PT periodic potentials," Physical Review Letters 100, 030402 (2008).
21. V. Achilleos, P. G. Kevrekidis, D. J. Frantzeskakis, and R. Carretero-González, "Dark solitons and vortices in PT-symmetric nonlinear media: From spontaneous symmetry breaking to nonlinear PT phase transitions," Physical Review A 86, 013808 (2012).
22. J. Paul, C. Christopoulos, and D. W. P. Thomas, "Generalized material models in TLM .I. Materials with frequency-dependent properties," IEEE Transactions on Antennas and Propagation 47, 1528–1534 (1999).
23. J. Paul, C. Christopoulos, and D. W. P. Thomas, "Generalized material models in TLM - part 3: materials with nonlinear properties," IEEE Transactions on Antennas and Propagation 50, 997–1004 (2002).
24. W. J. R. Hoefer, "The Transmission-Line Matrix Method--Theory and Applications," IEEE Transactions on Microwave Theory and Techniques 33, 882–893 (1985).
25. C. Christopoulos, The Transmission-Line Modeling Method TLM (IEEE Press, 1995).
26. S. Phang, A. Vukovic, H. Susanto, T. Benson, and P. Sewell, "Time domain modeling of all-optical switch based on PT-symmetric Bragg grating," in 29th Annual Review of Progress in Applied Computational Electromagnetics (Applied Computational Electromagnetics Society, 2013), pp. 693–698.
27. V. Janyani, A. Vukovic, and J. Paul, "The development of TLM models for nonlinear optics," Microwave review 10, 35–42 (2004).
28. V. Janyani, A. Vukovic, J. D. Paul, P. Sewell, and T. M. Benson, "Time domain simulation in photonics: A comparison of nonlinear dispersive polarisation models," Optical and Quantum Electronics 37, 3–24 (2005).
29. S. C. Hagness, R. M. Joseph, and A. Taflove, "Subpicosecond electrodynamics of distributed Bragg reflector microlasers: Results from finite difference time domain simulations," Radio Science 31, 931–941 (1996).
30. M. Bass, G. Li, and E. van Stryland, Handbook of Optics Vol. 4, 3rd ed. (McGraw Hill, 2010).
31. J. S. Aitchison, D. C. Hutchings, J. U. Kang, G. I. Stegeman, and a. Villeneuve, "The nonlinear optical properties of AlGaAs at the half band gap," IEEE Journal of Quantum Electronics 33, 341–348 (1997).
32. S. Lan, A. V. Gopal, K. Kanamoto, and H. Ishikawa, "Ultrafast response of photonic crystal atoms with Kerr nonlinearity to ultrashort optical pulses," Applied Physics Letters 84, 5124 (2004).